Fuel-lean ammonia/biogas combustion characteristics under the reacting swirl flow conditions

Guo Ren Mong[a], Meng-Choung Chiong[b,*], Cheng Tung Chong[c], Jo-Han Ng[d], Syed Mashruk[e], Manh-Vu Tran[f], Nor Afzanizam Samiran[g], Keng Yinn Wong[h], Agustin Valera-Medina[e]

[a] School of Energy and Chemical Engineering, Xiamen University Malaysia, 43900 Sepang, Selangor, Malaysia
[b] Department of Mechanical Engineering, Faculty of Engineering, Technology & Built Environment, UCSI University, 56000 Kuala Lumpur, Malaysia.
[c] China-UK Low Carbon College, Shanghai Jiao Tong University, Lingang, Shanghai 201306, China.
[d] Faculty of Engineering and Physical Sciences, University of Southampton Malaysia (UoSM), 79200 Iskandar Puteri, Johor, Malaysia.
[e] College of Physical Sciences and Engineering, Cardiff University, Wales, United Kingdom.
[f] School of Engineering, Monash University Malaysia, Jalan Lagoon Selatan, 47500 Bandar Sunway, Selangor, Malaysia.
[g] Department of Mechanical Engineering Technology, Faculty of Engineering Technology, Universiti Tun Hussein Onn Malaysia, 84600 Pagoh, Johor, Malaysia.
[h] School of Mechanical Engineering, Faculty of Engineering, Universiti Teknologi Malaysia, Skudai 81310, Johor, Malaysia.

Abstract

Ammonia has been identified as a viable energy vector for power generation. Using dual-fuel operation that mixes the ammonia with higher reactivity gaseous fuel can be vital in enhancing ammonia combustion. This study examined the fundamental swirl combustion characteristics of fuel-lean premixed ammonia/biogas via a numerical approach. The flame was established at an input thermal power of 7 kW and a global equivalence ratio of 0.8. The numerical model was verified and validated with biogas emissions data acquired through experimental work. At the 20 mm burner downstream, increased carbon dioxide mass fraction in the biogas lowered the peak flame temperature up to ~400 K. Moreover, the deformation of flame temperature radial profiles was also found aggravated as carbon dioxide concentration in the biogas elevated from 0% to 40%. The reduction in premixed reactant mixture reactivity not only initiated flame temperature profile deformation but also reduced the peak Damkhöler number significantly. The peak Damkhöler number was lowered by a factor of ~1.5 when carbon dioxide dilution in the biogas elevated by 40%. The premixed combustion was directed into the thin reaction flamelets zone with elevated carbon dioxide mass fraction, owing to the intensified flow fluctuation. This, in turn, gave rise to the average flow velocities, turbulent kinetic energy, and normalised turbulent flame speed, notwithstanding that heat release rate and laminar flame propagation declined. In all, the presence of carbon dioxide has been shown to lower the ammonia/methane mixture reactivity whilst escalating the reacting flow fluctuation.

Keywords: Ammonia; biogas; swirl combustion; premixed combustion; dual fuel

*Corresponding author
Address: Department of Mechanical Engineering, Faculty of Engineering, Technology & Built Environment, UCSI University, 56000 Kuala Lumpur, Malaysia.
Email: chiongmc@ucsiuniversity.edu.my ; mcchiong@outlook.com (MC Chiong)

1.0 Introduction

Carbon-free molecules like hydrogen (H_2) and ammonia (NH_3) are identified as potential substitutes for traditional carbon-based energy sources to mitigate global carbon emissions [1]. H_2 is an appealing carbon-free molecule, but its storage is challenging and pricey. On the contrary, the energy density of NH_3 is inherently greater than that of H_2. Furthermore, storage and transportation cost for NH_3 is also substantially more economic than for H_2 [2]. During the energy crises of the 1960s and 1970s, ammonia was temporarily used as transportation fuel [3]. Since the previous decade, initiatives to accelerate global carbon reduction have once more prioritised NH_3 as a viable alternative fuel, extending its use in direct-combustion-based power production and transportation fuel [2]. However, challenges are encountered when fuelling power generation machines with ammonia.

Due to ammonia's lower flammability than fossil fuels, it was shown that considerably greater ignition energy was needed to ignite the chemical [4]. At operation near the stoichiometric conditions, the minimum ignition energy for the NH_3/air mixture was ~21.5 times greater than the premixed propane (C_3H_8)/air mixture [5]. However, it was also observed that disassociated ammonia into hydrogen at ~28% could enhance the ammonia/air combustion, thus the minimum ignition energy was lowered by approximately two orders of magnitude [5]. Ammonia's flammability limit is likewise substantially narrower than that of H_2 and methane (CH_4). Methane and hydrogen can operate in a broader equivalence ratio (φ) range of 0.5-1.7 and 0.1-7.1, respectively. NH_3, however, can only operate within an equivalence ratio of 0.63-1.40 [6]. Owing to ammonia exhibiting lower flame stability than propane, a broader quenching distance is required for ammonia flame propagation at a global equivalence ratio of 0.8, a value that is around 50 mm broader than that for C_3H_8/air flame propagation [6]. To expedite ammonia as a greener fuel for upcoming power generation, elevating ammonia combustion quality along with minimal toxic emissions are crucial.

To enhance the combustion of neat ammonia, CH_4 was suggested as one of the potential solutions. Valera-Medina et al. [7] used a common swirl burner to study premixed NH_3/CH_4 combustion at various global equivalence ratios and CH_4 mass fractions. Global $\varphi > 1.25$ caused flame instability because the core recirculation zone was weaker. When $\varphi > 1.1$, the NO emission was very low (~20 ppm), mostly because amidogen radicals (NH_2^*) consumed most of the NO. On the other hand, carbon monoxide (CO) production was ~900 ppm when the global flame equivalence ratio exceeds 1.1. But in the fuel-lean combustion, reactions among the nitrogen atoms (N^*), imidogen (NH^*), and oxygen atoms (O^*), altogether with nitroxyl (HNO) + H (hydrogen atom) → NO + H_2, were identified as the main sources of NO production.

In another study, blending the NH_3 with CH_4 was reported to reduce NO production in the excess air operation to ~70 ppm/kW [7], which is substantially lower than the premixed combustion of ammonia/air where NO emission was ~151.5 ppm/kW [8]. When compared to the emissions performance of biodiesel, diesel, and natural gas, NH_3/CH_4 is still quite high [9,10]. Khateeb et al. [11] recently reported that when mixture input velocity and thermal power increased, the ammonia component in the fuel blend need to be reduced to ensure flame stability.

The non-premixed NH_3/CH_4 combustion under swirling flow and elevated atmospheric pressure conditions was studied by Somarathne et al. [12]. When the energy proportion of ammonia raised by 40%, The nitric oxide generation from NH_3/CH_4 non-premixed combustion surged by about three orders of magnitude. In another study [13], it was found that excess air non-premixed NH_3/CH_4 combustion resulted in encouraging NO mitigation. In contrast to premixed ammonia/air combustion, premixed ammonia/methane/air combustion lifted nitric oxide production by ~1.3 times. As opposed to non-premixed ammonia/air combustion, non-premixed ammonia/methane/air combustion lowered nitric oxide by a factor of ~2 [13]. Additionally, it was also unveiled that premixed ammonia/methane/air combustion produced

much greater nitrogen dioxide (NO_2) and nitrous oxide (N_2O) emissions than non-premixed ammonia/methane/air combustion. It was presumed that the main mechanism for NO generation during NH_3/CH_4 burning is due to fuel-bound nitrogen [13].

In a more recent study [14], the emission of premixed ammonia/methane/air swirl flames was examined numerically by elevating the NH_3 mole fraction up to 60%. The NO transport equation computed throughout the simulation is found to improve the NO emission. The study showed that residence period, temperature, and nitrogenous components are crucial determinants of NO concentration profile. For CH_4/NH_3 flames, the inner recirculation residence time determines the NO level, and locally high NO concentration is mostly driven by prolonged local residence time. The formation of OH^* and NO were tied to the high temperature [14]. The investigation of the radical components unveils that HNO is the primarily responsible for the important reaction route with regards to NO formation. The H, O, and O_2 concentrations declined as the NH_3 fraction was raised (leading to elevated HNO concentration). When the NH_3 mass fraction was increased to 40%, the NO production is the highest among all cases examined [14].

Zhang et al. [15] examined the blow-off features of NH_3/air and NH_3/CH_4/air swirl flames experimentally and numerically. The findings demonstrated that the ammonia swirl flame exhibited weak lean flame stability that may be significantly enhanced by incorporating CH_4 into the fuel. Furthermore, the lean blow-off limit for the NH_3 swirl flame does not appear to be affected by the elevated swirl number. On the other hand, the swirl number for the 50 wt.% NH_3 flame results in an obvious extension of the lean blow-off limit. Four distinct flame macrostructures responsible for eventual flame blow-off were identified when lowering the NH_3/air and NH_3/CH_4/air flame global equivalence ratio. In all, the NH_3/air flame extinguished much quicker than the NH_3/CH_4/air flame, which is mostly due to the excessive stretch that results in local extinction during the blow-off process [15]. Despite studies that are dedicated

to examine and understand the fundamental combustion characteristics of NH_3/CH_4/air swirl flames, the effects of carbon dioxide (CO_2) addition into NH_3/CH_4/air flame have not been analysed yet. CH_4 and CO_2 are the major components in a typical biogas mixture that is commonly produced via the anaerobic digestion of organic matter. Anaerobic digestion is widely recognised as a more environmentally friendly way of producing renewable methane. Considering the scarce understanding of NH_3/biogas swirl combustion, the present study aims to examine it numerically. By using NH_3/CH_4 swirl combustion as baseline, the flame temperatures, velocities, turbulent kinetic energy, premixed combustion regime, turbulent Damkhöler number (Da), and turbulent flame speed for NH_3/biogas swirl flame are examined.

2.0 Research method

2.1 Construction of swirl burner

Figure 1a depicts the schematic diagram of a swirl burner with the integration of premixed gas to improve flame stabalisation. The plenum was designed for the premixing of fuel and air to attain a homogeneous gaseous mixture, then transfer towards the swirler to be combusted. The reference for the exit plane of the burner is $h = 0\ mm$. The swirler hub has an internal diameter of 26 mm and an outer diameter of 40mm. The axial swirler comprises six straight vanes with a thickness of 1.5 mm and aligned 45° angle from the axial centerline axis, resulting in a geometric swirl number of roughly $S_N \sim 0.84$. The introduction of the swirl is to create a central toroidal recirculation zone (CTRZ) that enhances the mixing of combustion products with high thermal energy and unburned premixed reactants. This consequently promotes cleaner combustion whilst improving flame stabalisation. A quartz tube was placed on the exit plane's flange to visualise flames. The delivery system is depicted in Figure 1b. The dry air was delivered and controlled with a minimal deviation of 1.5% through a mass flow controller (Sierra). To replicate the biogas composition, CH_4 and carbon dioxide (CO_2) were delivered to the mixing chamber at a specific ratio. Mass flow controllers were employed to regulate the flow rate of CH_4 and CO_2 (Sierra, 1.5% full-scale accuracy). At the burner's exit, the mixture of air and fuel was ignited to establish the swirl flame.

2.2 Test procedures and operating conditions

Exhaust emissions like nitric oxide (NO), oxygen (O_2), and carbon dioxide (CO_2) were quantified by using a sampling probe connected to a gas analyser (KANE Quintox 905), and the sampling probe was placed 13 mm upstream from the quartz tube. The gas analyser can quantify NO, carbon monoxide (CO), O_2, and CO_2 in the ranges of 0-1000 ppm, 0-10,000 ppm, 0-25 %, and 0-99.9 %, respectively. The emission data were collected at five points radially

across the quartz tube outlet. By using the area-weighted average velocity approach [16], the mean average of all emissions was computed from the five points readings collected. For this study, a biogas composition of CH_4 (70 wt.%) blended with CO_2 (30 wt.%) was adopted. The flow rates of CH_4, CO_2, and air were configured to establish the swirl flame at an input thermal power of 7 kW and a global equivalence ratio of 0.8. The data collected was used for model verification and validation.

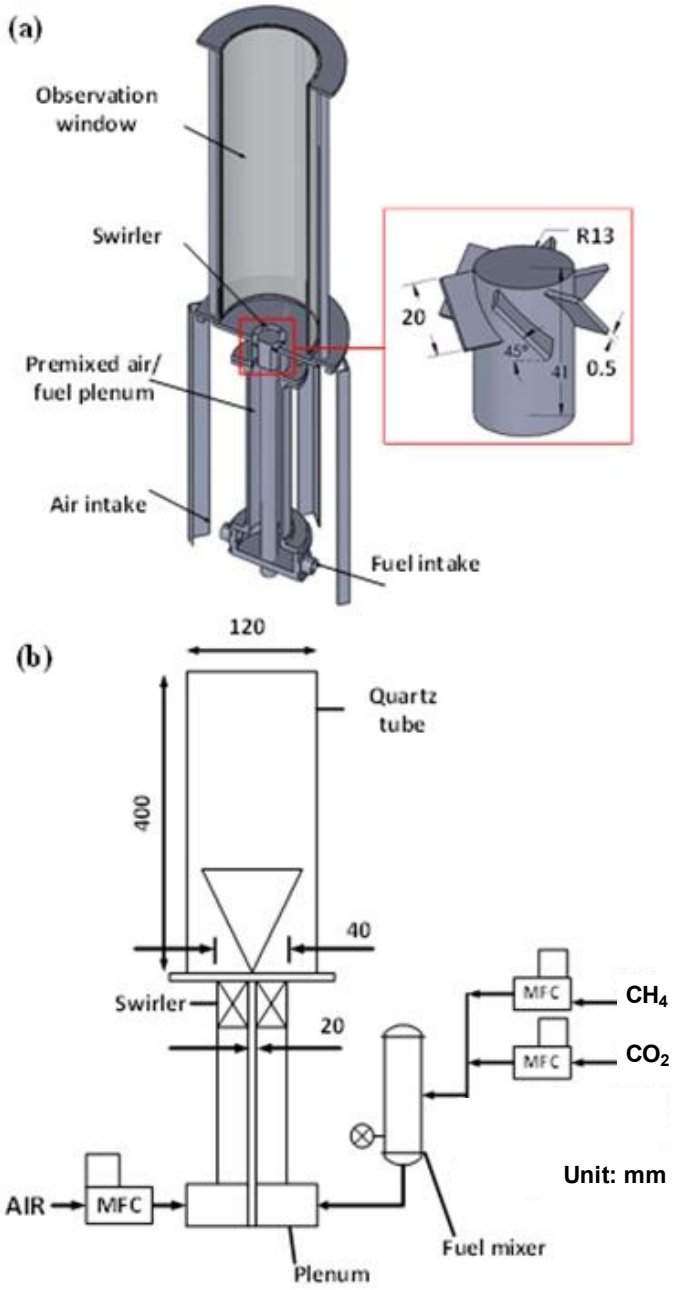

Figure 1 (a) The model of swirl burner and (b) schematic representation of the gas transport system. (Reprinted from [16] with permission from Elsevier)

2.3 Numerical modelling

2.3.1 Flamelet generated manifold (FGM)

The flamelet is simulated using a comprehensive chemistry reaction scheme in the FGM approach. The present work employed the Gas Research Institute mechanism (GRIMECH 3.0 - GRI 3.0) scheme (53 species, 325 reactions) as a chemical kinetics reaction mechanism. The FGM technique employs the chemistry from a laminar flamelet database built from many 1D flamelet computations done with full chemical kinetics and transport equations. The type of flamelet (premixed or non-premixed) is decided based on the boundary conditions of each flamelet, which vary somewhat. The premixed swirl flame was modelled in this work with the software - ANSYS Fluent. A one-dimensional premixed flamelet was constructed to solve the flamelets in reaction progress space. The following equation defines the variable reaction progress:

$$c = \frac{[\sum_k \alpha_k (Y_k - Y_k^u)]}{[\sum_k \alpha_k (Y_k^{eq} - Y_k^u)]} = \frac{Y_c}{Y_c^{eq}} \quad (1)$$

The progress variable is defined as a normalised sum of the mass fraction of the product species across all species in the chemical process. From equation (1), Y_k represents the mass fraction of the k^{th} species, u represents the unburned reactant at the flame input, and eq represents chemical equilibrium at the flame exit. Accordingly, the coefficient α_k is provided so that the flame's reaction rate, c, grows monotonically. $\alpha_k = 0$ for all species, with the exception of $\alpha_{CO_2} = \alpha_{CO} = 1$ for hydrocarbon combustion and $\alpha_{H_2O} = 1$ for fuels containing no C element, such as H_2. The adiabatic flamelet equations in one dimension can be translated from physical-space to reaction-progress space.

$$\rho \frac{\partial Y_k}{\partial t} + \rho \frac{\partial Y_k}{\partial c} \dot{\omega}_c = \rho \chi_c \frac{\partial^2 Y_k}{\partial c^2} + \dot{\omega}_k \quad (2)$$

196 $$\rho\frac{\partial T}{\partial t}+\rho\frac{\partial T}{\partial c}\dot{\omega}_c=\rho\chi_c\frac{\partial^2 T}{\partial c^2}-\frac{1}{c_p}\sum_k h_k\dot{\omega}_k+\frac{\rho\chi_c}{c_p}\left(\frac{\partial c_p}{\partial c}+\sum_k c_{p,k}\frac{\partial Y_k}{\partial c}\right)\frac{\partial T}{\partial c} \quad (3)$$

197 where Y_k is the k^{th} species mass fraction, T is the temperature, ρ is the density of the
198 fluid, t is time, $\dot{\omega}_k$ is the k^{th} species mass fraction rate, h is the total enthalpy and $c_{p,k}$ is the
199 k^{th} species specific heat at constant pressure. The definition of the scalar dissipation rate χ_c is:

200 $$X_c=\frac{\lambda}{\rho c_p}|\nabla c|^2 \quad (4)$$

201 Where λ corresponds to heat conductivity. Variable with c, the scalar dissipation χ_c is
202 an input to the equation set, where Equation 4 corresponds to:

203 $$\rho\frac{\partial Y_k}{\partial t}+\rho\frac{\partial Y_k}{\partial c}\dot{\omega}_c=\frac{\lambda}{c_p}|\nabla c|^2\frac{\partial^2 Y_k}{\partial c^2}+\dot{\omega}_k \quad (5)$$

204 Other than the progress variable, the mixture fraction in FGM corresponds directly to
205 the single equivalence ratio of the 1D premixed flamelet. The maximum scalar dissipation,
206 χ_{max}, of a premixed flamelet at varying mixture fractions is distinct. Modelling the scalar
207 dissipation $\chi_c(f,c)$ at any mixture fraction f as

208 $$\chi_c(f,c)=\chi_{max}^{STO}\exp\left(-2\left(\text{er fc}^{-1}\left(\frac{f}{f_{STO}}\right)\right)^2\right)\exp\left(-2\left(\text{er fc}^{-1}(2c)\right)^2\right) \quad (6)$$

209 where *STO* represents the stoichiometric proportion of the mixture and $er\,fc^{-1}$is the
210 inverse complimentary error function. The only model input to the premixed flamelet generator
211 in ANSYS Fluent is the scalar dissipation at stoichiometric mixture fraction, X_{max}^{sto}. The
212 solution of unstrained (freely propagating) physical space flamelets for rich, lean, and
213 stoichiometric hydrocarbon and H_2 flames at standard temperature and pressure [16] often
214 matches the default value of $X_{max}^{sto}=1000/s$ s.

215

2.3.2 Grid setup

To achieve a reliable simulation result, the numerical grid setup is vital. Location with high temperature and possible species concentration requires high-quality components with a slow development rate. As depicted in Figure 2, the cut shell approach, which largely comprises of a structured hexahedron grid, was selected for this simulation investigation. The minimum and the maximum number of cells in the grid are 0.7 and 1 million, respectively. Aspect ratio and orthogonal quality determined the quality of the mesh. According to Zerrin et al. [17], a hexahedron grid with a maximum aspect ratio of 35 and a minimum orthogonal quality of 0.15 is of high quality. In this instance, the highest aspect ratio was 13.43 and the minimum orthogonal quality was 0.19, which falls within the range specified by Zerrin and colleagues [17]. Near the burner outlet, a denser grid of cells was formed, while the grid grew coarser as it approached the burner outlet. At the exit of the burner, a refined mesh is required to predict the occurrence of high velocity, species, and temperature gradient.

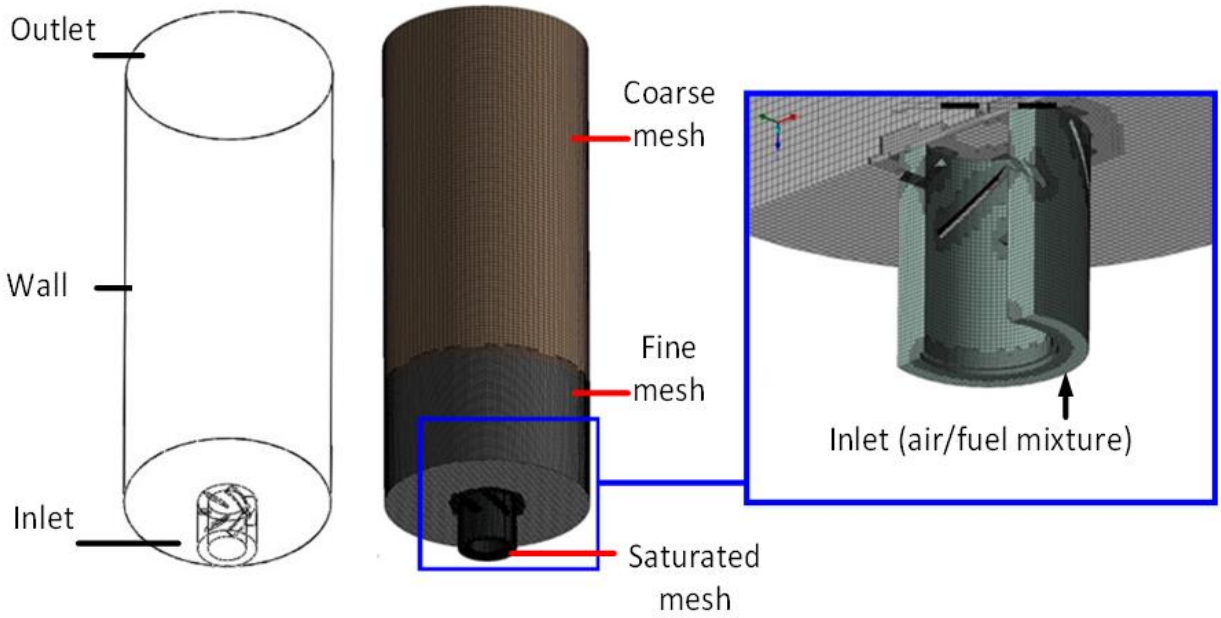

Figure 2 The simulation setting of boundary conditions and mesh setup. (Reprinted from [16] with permission from Elsevier)

2.3.3 Fuel compositions and boundary conditions

As stated in Table 1, several biogases/ammonia compositions were used as operational fuels in this simulation. Based on these compositions, a mass flow rate model setup was built at the inlet. Simulations were performed at an input thermal power of 7 kW and φ = 0.8. The turbulence intensity and hydraulic diameter at the fuel input were set to 5% and 10 mm, respectively. The turbulence intensity value is derived from the value indicated by Krieger, et al. [18]. The combustor wall was assumed to be a no-slip boundary and species flux is absent. Flow outlet at the exit of the burner was regarded as the burner outlet condition. At the outlet boundary, the static pressure was set to atmospheric surrounding pressure.

Table 1 CH_4, CO_2, and NH_3 mass fraction in the premixed biogas/NH_3.

Biogas composition		**NH_3 wt.% in biogas/NH_3 mixture**	**Acronym**
CH_4 wt.% in biogas	**CO_2 wt.% in biogas**		
100%	0%	20%	C0N20
100%	0%	30%	C0N30
100%	0%	40%	C0N40
70%	30%	20%	C30N20
70%	30%	30%	C30N30
70%	30%	40%	C30N40
60%	40%	20%	C40N20
60%	40%	30%	C40N30
60%	40%	40%	C40N40

2.3.4 Convergence criteria

The grid independence test was performed using various numbers of elements, as shown in Figure 3a. The NO emissions for biogas converges at 1.7 million elements, irrespective of the variation in global equivalence ratio from 0.9 to 0.75. The grid number of 1.7 million was deemed grid-independent since the results were nearly comparable to those of the >1.8 million scenario. Several criteria reported by earlier scholars were used to determine the convergence of a solution. Mayr et al. [19,20] claim that the simulation is deemed to converge if the fluctuations of maximum temperature is <5 K and species concentration is <0.001 mol fraction. The residuals for mixture fraction variance and mean mixture fraction should be reduced to less than 10^{-6}, whereas the residuals for other equations, such as continuity, velocity, and k-epsilon are less than 10^{-3} [19,20]. In addition to residual, the number of iterations is also an indicator of the convergence of simulation process. As depicted in Figure 3b, the variations in NO emission have no obvious changes after 5000 iterations. As the NO value fluctuates minimally and enters a steady state, the NO_x mean value is regarded to have converged. Figure 3c and Figure 3d show that flame shape obtained via numerical simulation resemble that captured during the experimental work. A notable feature in 2D swirl flame image is the formation of High Momentum Flow Region (HFMR) at burner outlet. Such feature is also shown in previous studies involved swirl flames [16,21].

2.3.5 Fluid flow modelling

The mass, momentum, energy, and heat transfer equations were solved in this investigation using ANSYS Fluent with finite volume. For steady-state conditions, a pressure-based solver was utilized. Solving the RANS (Reynold-averaged Navier Stokes) equations describes the fluid flow. To close the RANS equations, turbulence models were used. In the Computational Fluid Dynamics (CFD) code, several turbulence models are provided. The

standard k- model was used for the turbulence model in this simulation. The pressure-velocity coupling was calculated using a SIMPLE computational technique [19,20]. The governing equations for momentum, turbulent kinetic energy and dissipation rate, progress variable, and mixture fraction are discretised using a second-order upwind approach. The PRESTO! system is implemented for pressure. Mayr et al. [19,20] reported that the PRESTO! technique expedites simulation convergence.

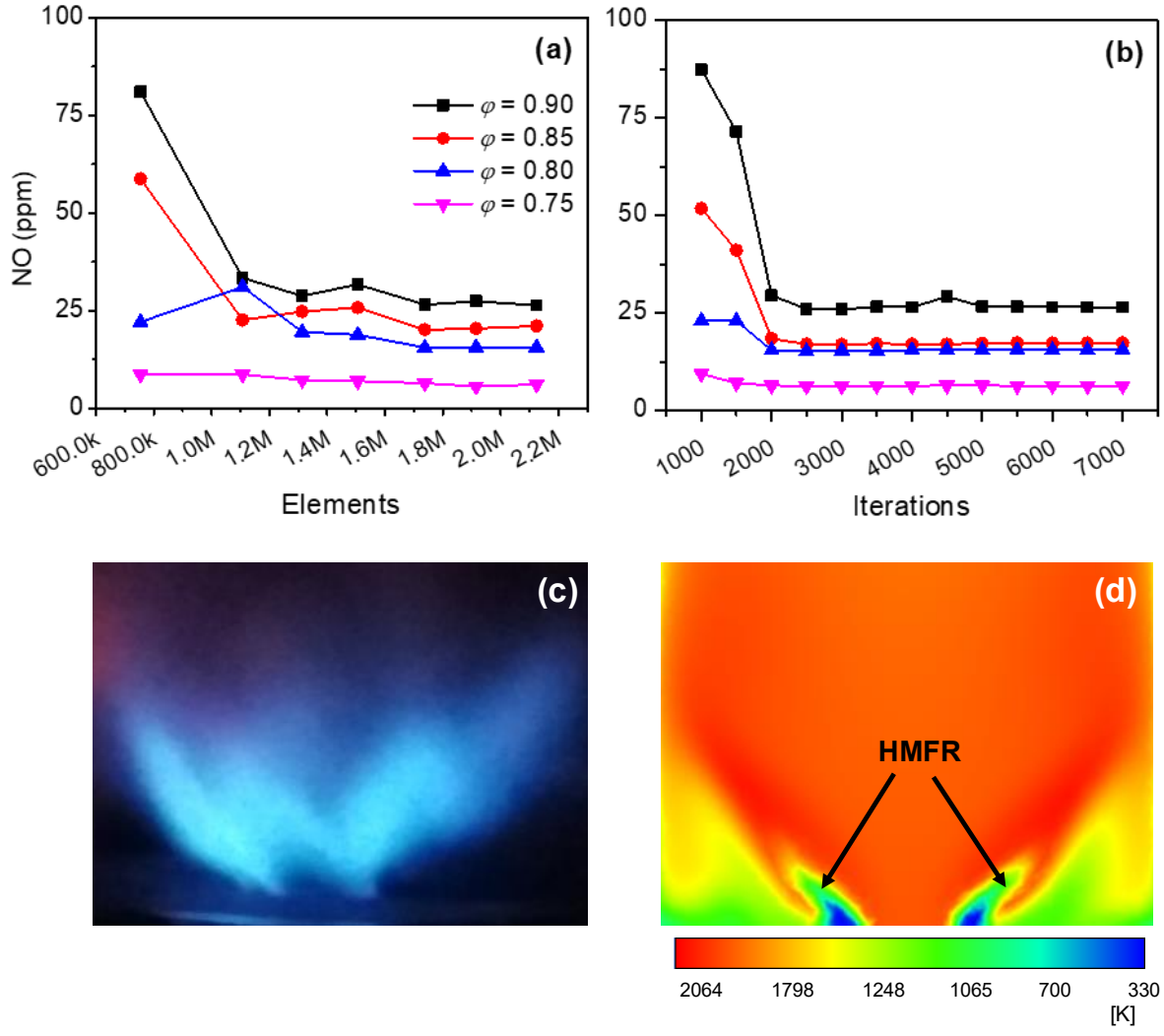

Figure 3 Emission of NO from biogas at 7 kW input thermal power as a function of (a) grid or mesh element size, and (b) the number of iterations. Biogas swirl flame images (7 kW input thermal power, φ = 0.8) obtained via (c) experiment, and (d) numerical simulation.

Figure 4a compares the experimental data with the estimated NO emissions by the FGM models at various equivalence ratios. It has been noted that the FGM-estimated NO concentration exhibits a tendency that is comparable to that of experimental data. At lean regions, prediction by the FGM technique demonstrated good agreement with experimental results, particularly at equivalence ratios of 0.85 and below. However, when stoichiometry was approached, the concentration of NO was much over anticipated. A similar trend was also observed by [16]. Premixed FGM's divergence from experimental data is mostly attributable to the species' inability to disseminate in the direction of the Z gradient. Thus, one of the variables causing the variation in NO concentration is the absence of the diffusion effect in the premixed FGM model [22].

As can be shown in Figure 4b, the deviation of the CO_2 species predicted by the FGM model from the actual experimental value is often less than 10%. However, when the equivalency ratio becomes closer to stoichiometric, the FGM technique underestimates the CO_2 emissions. According to Najafi-Yazdi et al. [23], the mass fraction is decomposed before considerable heat release, hence the progress variable frequently produces erroneous findings for rich mixes. Figure 4c demonstrates that the FGM technique accurately predicts the O_2 species since the error percentage is less than 10% for all equivalence ratios. For quick chemical processes, the FGM technique primarily use quasi-steady state approximation, and this method is ideally suited to forecast free radical species like O_2 [24].

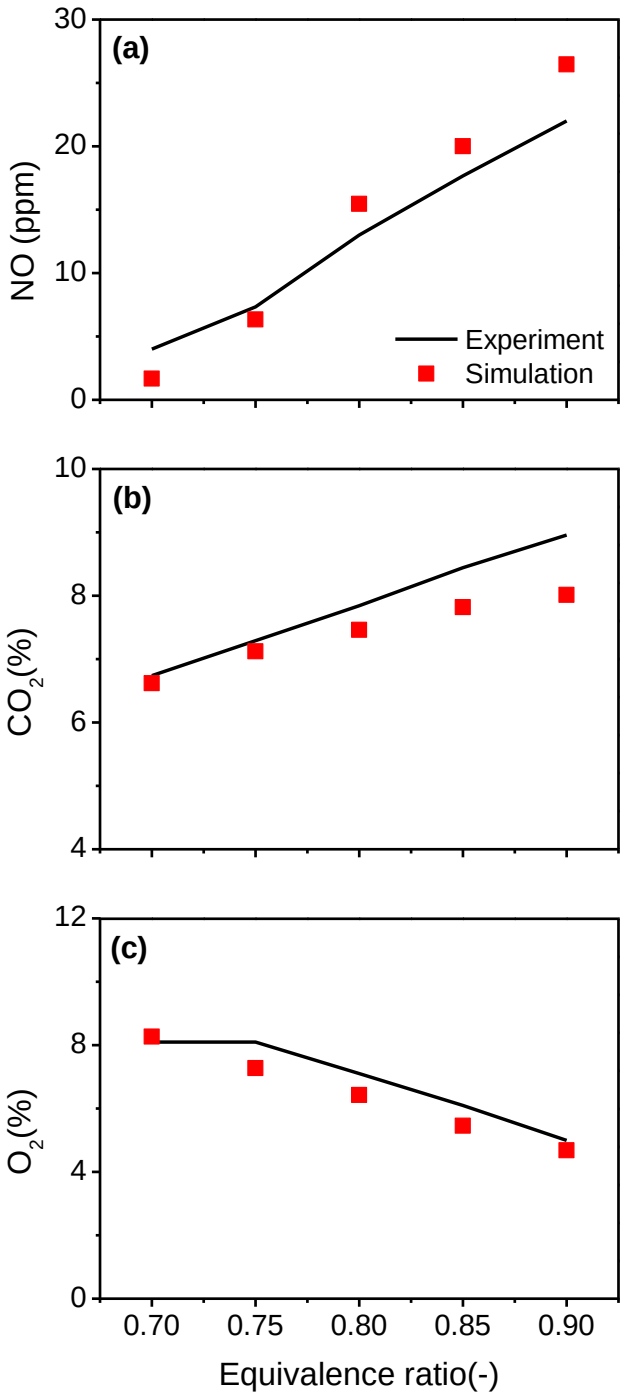

Figure 4 (a) NO, (b) CO_2, and (c) O_2 emissions of biogas combustion at 7 kW input thermal power obtained from experiments and numerical simulations using FGM method as a function of equivalence ratio.

3.0 Result and discussion

Figure 5a shows that for the fuel mixture with 20 wt.% NH_3, the flame temperature reduces by averaging 150 K as CO_2 wt.% increases from 0% to 40% at 20 mm downstream. In addition to the flame temperature reduction, the peak temperature is also shifted radially outwards, and the dual temperature peak are apparent when CO_2 wt.% increases to 40%. A similar temperature profile deformity is advanced to a lower CO_2 wt.% when NH_3 wt.% in the reactant increases to 30% and 40%, as shown in Figure 5b and Figure 5c. Figure 6 illustrates the dual peak temperature by comparing flame temperature profiles with normalised OH^* intensity. It is shown that the peak OH^* is present at nearly the same location where the temperature peak is found (C0N40). With elevated CO_2 mass fraction, dual peak OH^* is formed and aligns with the radial position of dual peak temperature.

For fuel mixture without CO_2 infusion (i.e., C0N20, C0N30, and C0N40), peak temperature takes place at a radial position ~35 mm for 20 mm downstream, regardless of the variation in NH_3 mass fraction. Thus, the displacement of peak temperature to an outer radial position at elevated CO_2 wt.% suggests that a portion of the premixed reactant mixture is not consumed at the inner branch of the reaction zone. Conversely, it is carried to an outer branch of the reaction zone by the positive radial velocity of the swirling flow. At 30 mm downstream (Figure 5d-f), the peak temperature for all fuel mixture is stretched radially by another ~5 mm. This is primarily due to the expansion of the swirling flow diameter farther downstream. Meanwhile, increased NH_3 mass fraction in the absence of CO_2 (i.e., C0N20, C0N30, and C0N40) does not result in dual peak temperature at 20 mm downstream. This denotes that CO_2 is the main contributor to the dual peak temperature formation, seemingly because of CO_2 decelerates the reaction rate that hinders the establishment of uniform reaction across the HFMR. At 30 mm downstream (Figure 5d-f), the dual peak temperature diminishes despite the radial displacement of peak temperature remains illustrious. The shifting of peak temperature

to the outer branch and the existence of multiple reaction zones due to the addition of secondary fuel were also observed in a study pertaining to n-heptane/natural gas dual fuel swirl flame [25]. The flame peak temperature at a 15 mm burner downstream was split up and shifted by ~5 mm radially outwards when natural gas was added to the n-heptane swirl flame. Moreover, the dual peak was also seen in the normalised OH^* signal at 5 mm and 15 mm downstream, respectively. For neat n-heptane swirl flames, however, no double peak temperature was observed [25]. Premixing the CO_2 into the CH_4/NH_3 blend has resulted in notable change in flame temperature radial profiles, especially at near burner outlet. The addition of CO_2 tends to stretch the peak temperature radially outwards and demands an extended downstream distance to develop a more uniform reaction radially across the HMFR.

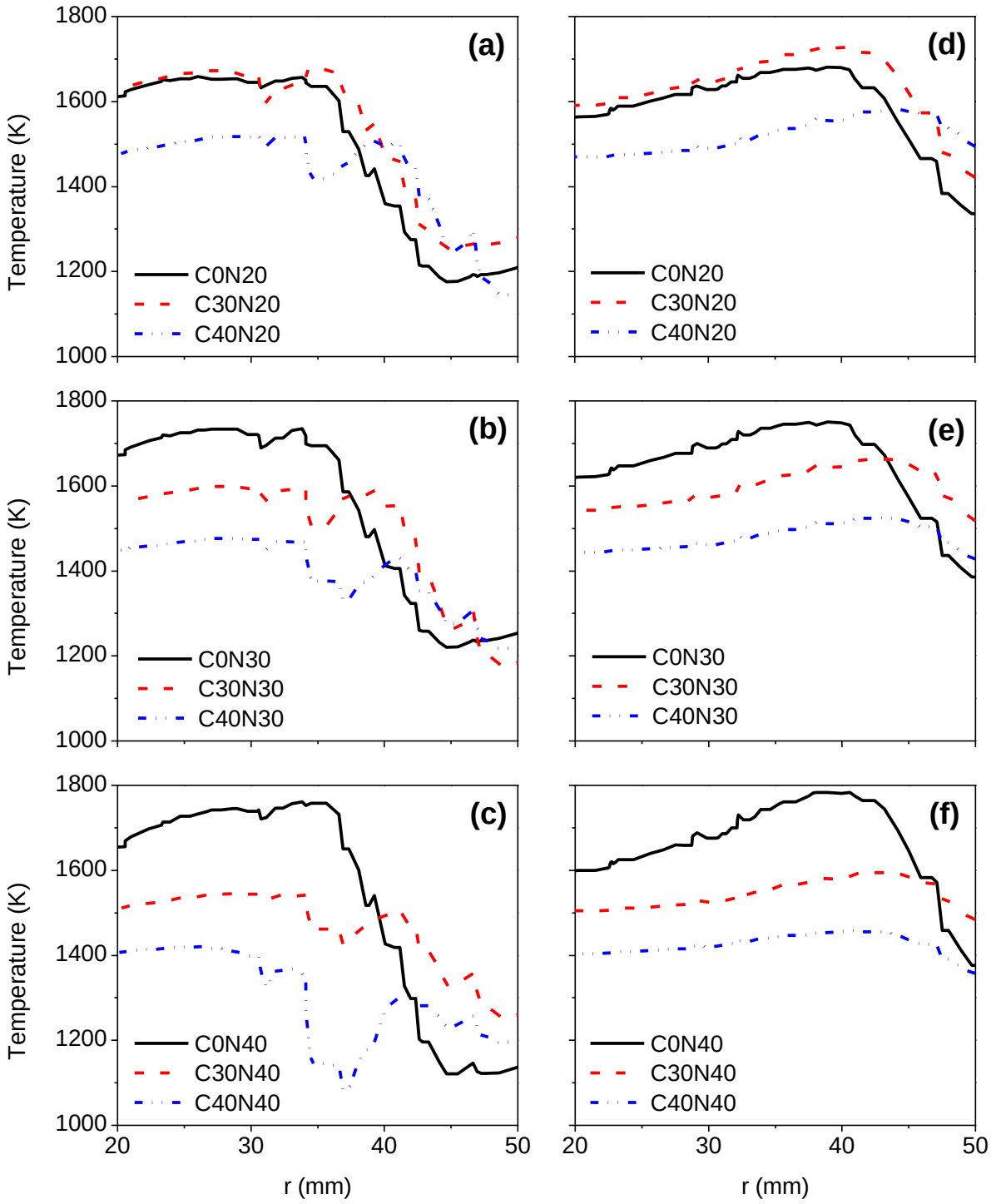

Figure 5 Flame temperature radial profiles for $CH_4/NH_3/CO_2$ premixed combustion (7 kW input thermal power, φ = 0.8) at (a-c) 20 mm, and (d-f) 30 mm downstream from the burner outlet.

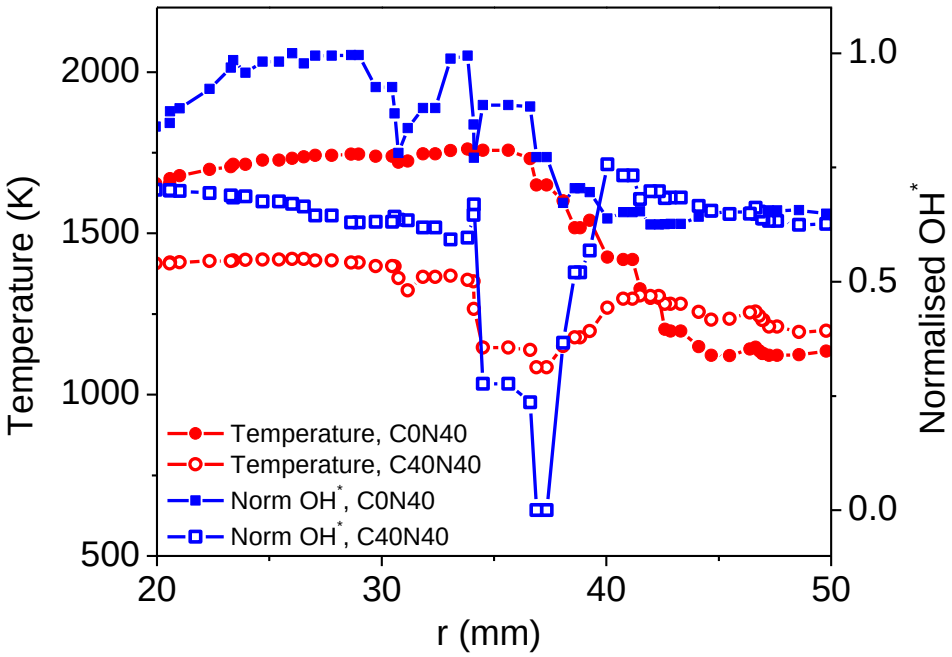

Figure 6 Normalised OH^* and temperature radial profiles for $CH_4/NH_3/CO_2$ premixed combustion (7 kW input thermal power, φ = 0.8) at 20 mm downstream from the burner outlet.

Figure 7 shows that peak velocities (axial, radial, and tangential) are concentrated within the HMFR. It can be observed also that the peak velocities for fuel mixture with 40 wt.% CO_2 is overall higher than 0% CO_2 by averaging 6 m/s, irrespective of the variation in NH_3 mass fraction. The introduction of CO_2 has also altered the size and turbulent kinetic energy of the structure as depicted in Figure 8, whereas the turbulent kinetic energy for the CH_4/NH_3 is notably lower than the CO_2-infused fuel mixtures. Increased CO_2 mass fraction not only elevates turbulent kinetic energy, but it also shifts peak turbulent kinetic energy and velocities radially outward by ~10 mm.

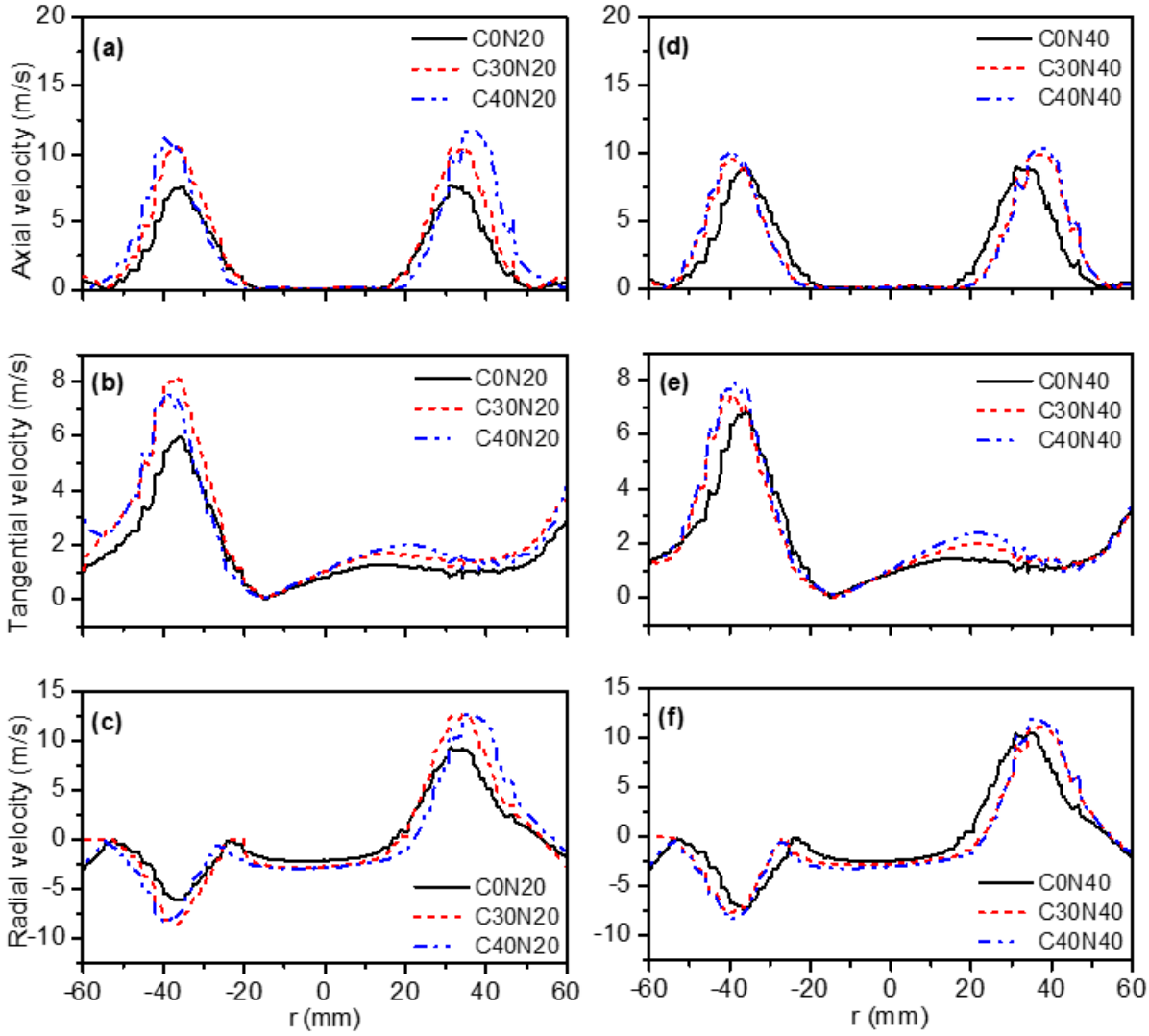

Figure 7 Velocities profiles of $CH_4/NH_3/CO_2$ premixed combustion (7 kW input thermal power, φ = 0.8) at 20 mm downstream from the burner outlet.

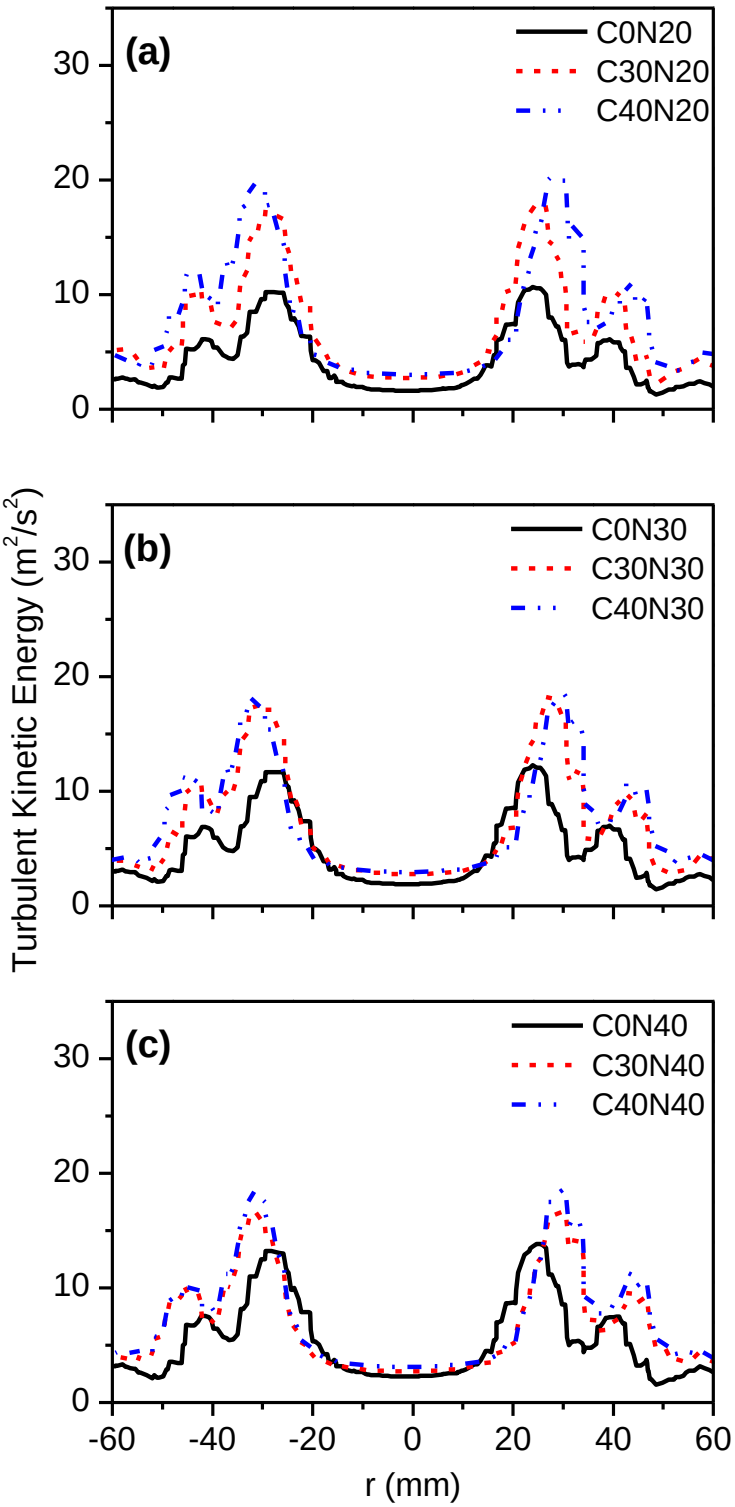

371

372 Figure 8 Turbulent kinetic energy for $CH_4/NH_3/CO_2$ premixed combustion (7 kW input thermal
373 power, φ = 0.8) at 20 mm downstream from the burner outlet.

374

375

With reference to Figure 5, increased CO_2 wt.% leads to an averaging lower flame temperature, owing to the less released chemical energy. Thus, the elevation of gas velocities and turbulent kinetic energy due to the increased CO_2 wt.% are apparently not because of the increased heat release rate. As illustrated in Figure 9, increased CO_2 wt.% directs the premixed combustion into the thin reaction zone where the fluctuation is becoming more prominent than flame laminar propagating speed. Aggravated flame fluctuation leads to the persistent local flame quenching and reignition. The eddies of premixed reactant mixture that receive an influx of heat from active species are ignited and burned irregularly, depending on the eddy size and local mixture composition [26]. This promotes the formation of a combustion wave that consequently gives rise to the gas velocities and turbulent kinetic energy as indicated in Figure 7 and Figure 8, respectively. The O_2/CO_2 volumetric ratio has consequential effects on flame fluctuation. As O_2/CO_2 decreased from 35% to 31% (i.e., increased CO_2 volume fraction in the premixed reactant), the heat release fluctuation for a CH_4 swirl flame increased by ~90% [27]. Although lowering the O_2/CO_2 to < 31% resulted in relative peak fluctuation amplitude reduction by ~40%, this was accompanied by a wider band peak with multiple peaks resided, denoting the flame started to fluctuate at a wider bandwidth prior to its extinction at 21% O_2/CO_2 volumetric ratio [27]. Increased CO_2 wt.% in the premixed reactant mixture tends to provoke flame fluctuation, and this basically promotes the development of a combustion wave which in turn raises the gas velocities and turbulent kinetic energy.

Figure 7 also shows that radial velocity has reduced noticeably when landing on the left-hand side of the reaction zone. The radial velocity on the right is ~12 m/s, decreasing its value on the left to ~8 m/s, a reduction of ~33%. On the contrary, the tangential velocity at the left-hand side of the reaction zone is remarkably higher than that at the right, showing an energy tradeoff between radial and tangential velocities in the flow field whereby the radial flow momentum is transferred to raise tangential velocity that consequently set up the swirl flow

motion to anchor the flame right at the top of the burner outlet. In other study [28], the axial velocity gradient increased notably right at the vicinity of Central Toroidal Recirculation Zone (CTRZ) and the HMFR on the right-hand side of the swirl flame, but its magnitude on the left-hand side of the swirl flame was ~50% lower than that of the right-hand side, signifying flow momentum exchange in the swirling flow field [28].

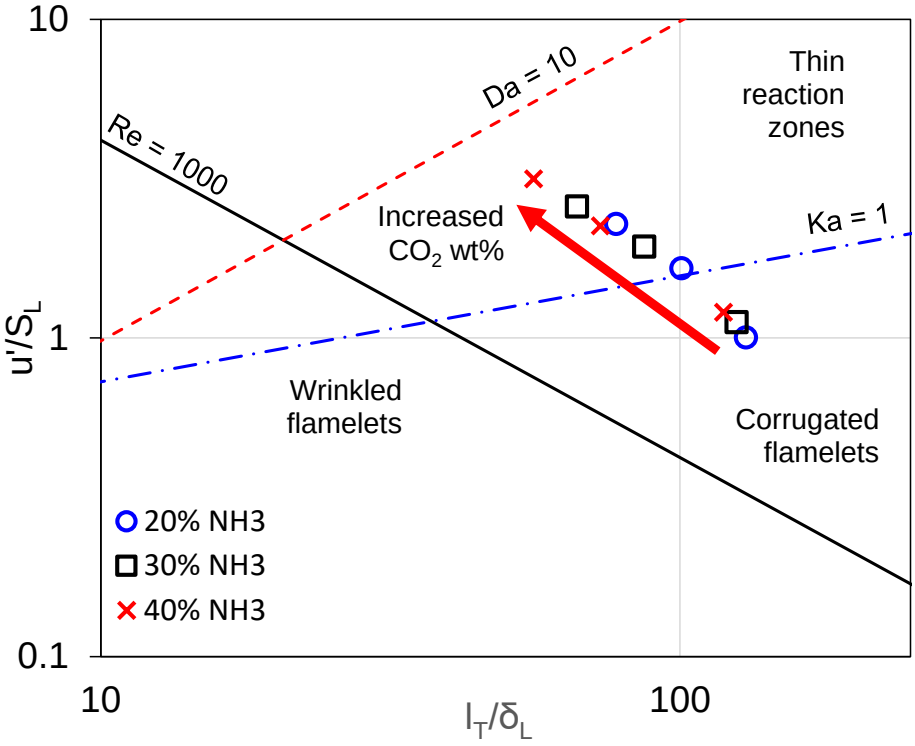

Figure 9 Regimes of $CH_4/NH_3/CO_2$ premixed turbulent combustion (7 kW input thermal power, φ = 0.8) in the Borghi diagram.

Figure 10 shows that the turbulent Damkhöler number for the methane/ammonia is considerably higher than the premixed reactant mixture with 30 wt.% and 40 wt.% CO_2 by ~40%. In all cases, notably high Da takes place at the central region of the reaction zone and declines radially outwards. The increase in length scales of the flame and the fall in turbulence intensity cause the Da to grow in the central region. Increased length scales of the flow are reflected in Figure 7 where flow velocities are minimal in the central region of the reaction zone. The length scales decline near the boundary of CTRZ and HMFR, owing to the elevated turbulent intensity in this region and this, in turn, lowers the Da [26]. O'Doherty and Gardner [28] study on swirling flow demonstrated that a wide range of eddies appeared in the vicinity of the CTRZ and the HMFR. These eddies promote rigour mixing and at the same time elevate turbulent intensity in this region [28].

Meanwhile, increased CO_2 wt.% reduces the Da drastically at the central region of the combustor, this is mainly because of the substantial reduction in laminar flame speed with increasing CO_2 mass fraction (Figure 11b). A similar tendency is also observed when the NH_3 mass fraction is raised, owing to the decline in the laminar flame speed and increased flame thickness. Owing to the lower NH_3/air burning rate, the thickness of the reaction zone for NH_3/air stoichiometric laminar flame under atmospheric conditions is wider than CH_4/air by a factor of approximately 12 [6]. A secondary peak of Da is observed at the near-wall area, despite it is considerably lower than Da at the central region. Like the central region, the Da for methane/ammonia is distinctively higher than the premixed reactant mixture with CO_2 infusion. The elevation of CO_2 mass fraction in the premixed methane/ammonia fuel mixture has inherently led to a significant reduction in Da, mainly due the decline in mixture reactivity.

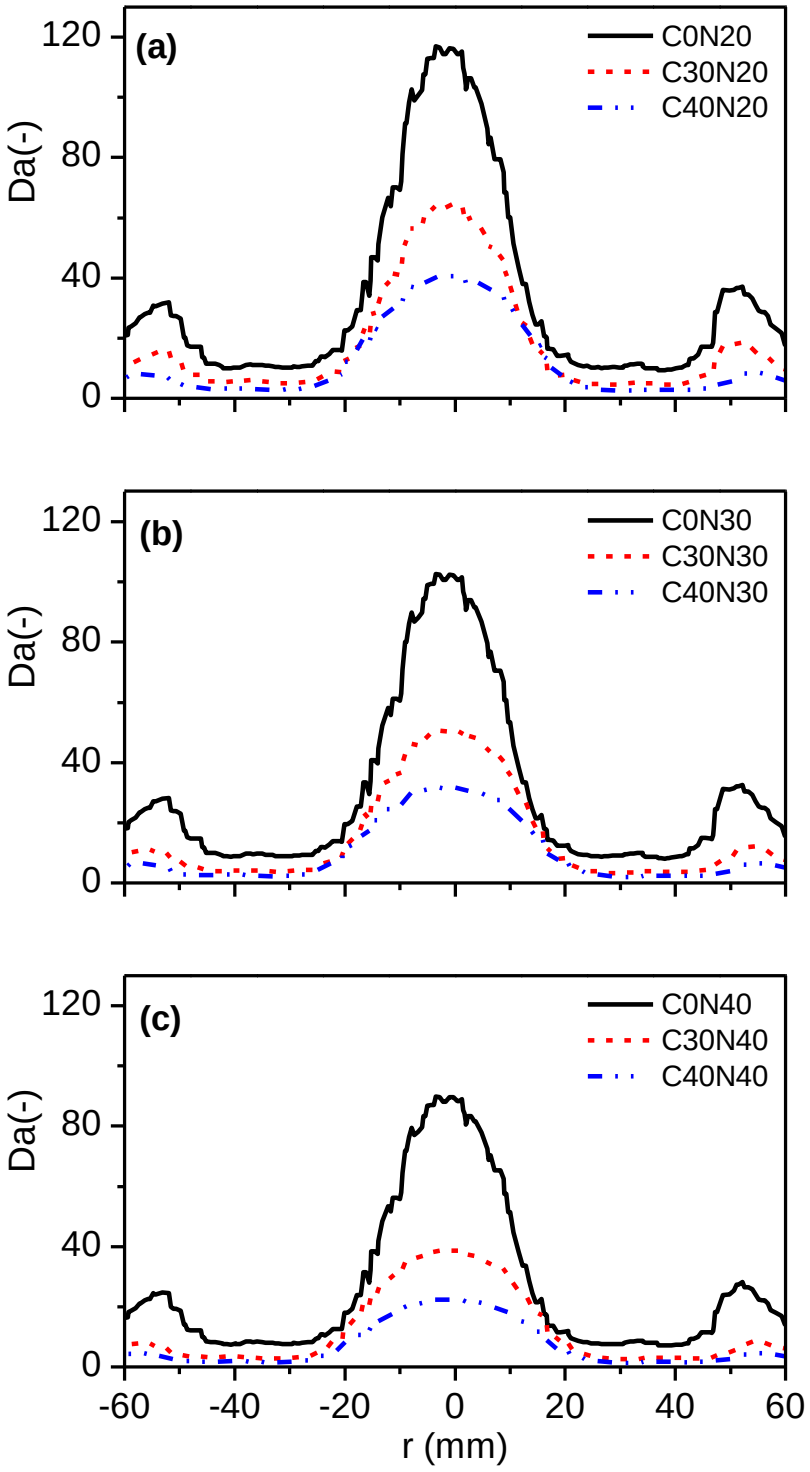

436

437 Figure 10 Da radial profile for $CH_4/NH_3/CO_2$ premixed combustion (7 kW input thermal power,
438 φ = 0.8) at 20 mm downstream from burner outlet.

439

440

441

442

Figure 11a illustrates that normalised turbulent flame speed increases in a linear fashion with normalised turbulent intensity below 1.5. As normalised turbulent intensity goes beyond 1.5, the increase of normalised turbulent flame speed turns out to be somewhat steeper. Furthermore, CH_4/NH_3 mixture with a higher CO_2 mass fraction results in a noticeably higher normalised turbulent flame speed than a fuel mixture with a lower CO_2 mass fraction. Likewise, increased NH_3 mass fraction also leads to an increased normalised turbulent flame speed when the CO_2 mass fraction in the fuel mixture is fixed. Elevated normalized turbulent flame speed is postulated because of the magnified combustion pulsation when CO_2 and NH_3 mass fractions are escalated. As shown in Figure 9, the wrinkling flamelet is diminishing with higher levels of turbulent intensity. The idea of a coherent flame front would no longer be valid in this case, and the combustion is preserved almost exclusively by the reactions established at the interface of fresh mixture' eddies and hot combustion active species. Depending on the composition of the mixture and the magnitude of the local turbulence intensity, the flow of heat and active species consume each eddy at an irregular rate. Intensified flow pulsations are produced in this way, elevating the gas flow velocities and turbulent flame speed as a result. The influence of small turbulent eddies are consequential, it was demonstrated that when the proposed numerical model considered small turbulent eddy effects on the flame front, the estimated turbulent flame speed was more closely matched to the measured values, indicating the significance of small-scale turbulent eddies that enter the preheating layer of the premixed flame front in affecting the normalised turbulent flame speed [29]. A fragmented flame front at higher turbulent intensity generates pressure pulsation that overall elevates the normalised turbulent flame speed.

Figure 11b, however, shows that the laminar flame speed declines with the rise of turbulent intensity. This ascertains that the increased S_T/S_L in Figure 11a is predominantly because of the exaggerated flow pulsations but not because of the increased reactivity when turbulent intensity is amplified. The reduction in S_L, on the other hand, can be attributed to the

flame stretching as flow momentum increased especially in the fuel-lean operation. The flame surface for the fuel-lean CH_4/air premixed turbulent flame was found to expand by a factor of approximately 3 as Reynolds number (Re) was raised by an order of magnitude [30]. With inflated flame stretching, the heat loss turns out more prominent than heat generation, and this leads to the laminar flame speed reduction as a result.

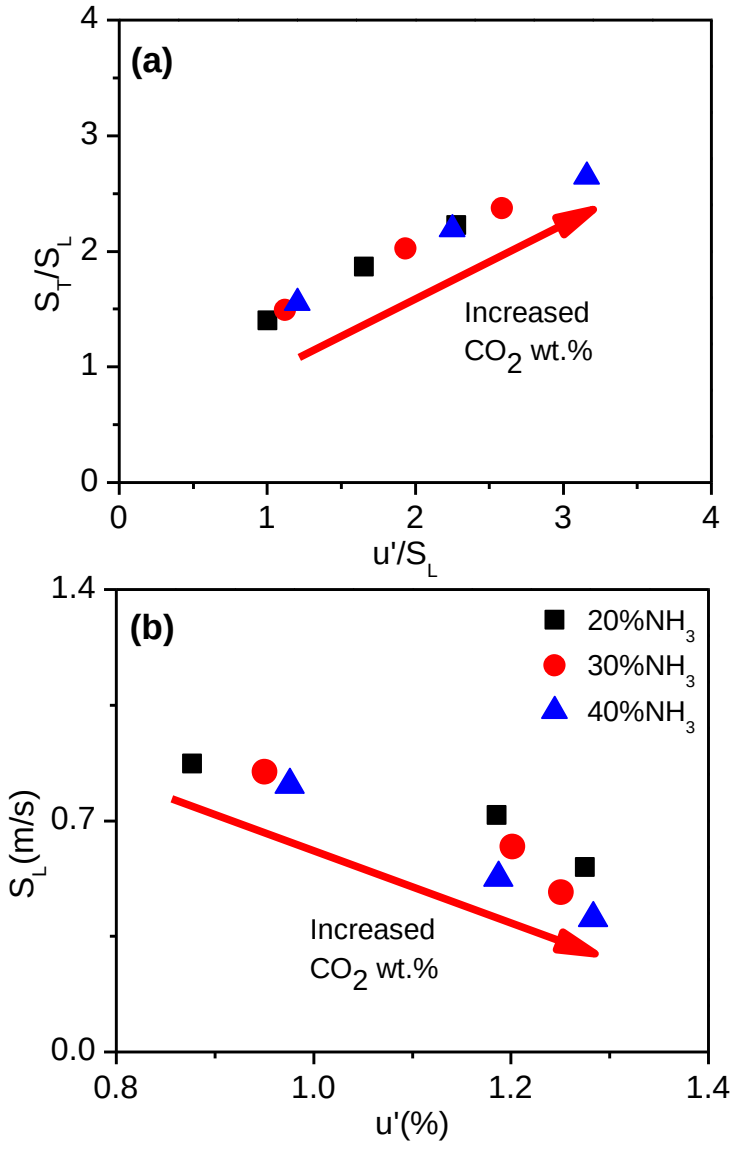

Figure 11 (a) Normalised turbulent flame speed vs normalised turbulent intensity, and (b) Laminar flame speed vs turbulent intensity for $CH_4/NH_3/CO_2$ premixed combustion (7 kW input thermal power, φ = 0.8).

4.0 Conclusion

The fundamentals swirl combustion characteristics of CH_4/NH_3 under elevated CO_2 addition and at a global equivalence ratio of 0.8 were examined. A commercial CFD package was employed to model the flow domain and simulate the physics of the reacting swirl flow. The numerical results were verified and validated using emissions data obtained via in-house experimental works. This study unveils that the introduction of CO_2 has profound effects on CH_4/NH_3 combustion characteristics. Increased CO_2 mass fraction to 40 wt.% in the premixed CH_4/NH_3 mixture lowers the peak flame temperature by 150-400 K on average as compared to the 0 wt.% CO_2 case. Moreover, the peak temperature is stretched by ~5 mm radially outwards and visible radial temperature profile deformation is observed particularly in the upstream region. These are mainly due to the reduction in reactivity of the premixed reactant mixture with elevated CO_2 wt.%. The reduction in mixture reactivity is also reflected in the peak Da reduction by a factor of ~1.5 when CO_2 wt.% increases from 0% to 40%.

Furthermore, increased CO_2 wt.% also directs the premixed combustion from corrugated flamelet into thin reaction flamelet, primarily because of the turbulent fluctuation has prevailed over the laminar flame propagation significantly. Increased flow pulsation due to the elevated CO_2 wt.% raises the flow velocities and turbulent kinetic energy visibly. Furthermore, aggravated flow pulsation also has a prominent effect on turbulent flame propagation. Despite a drastic reduction in laminar flame speed, the normalised turbulent flame speed has increased by a factor of 1.6 when CO_2 wt.% is raised from 0% to 40%, corresponding to an increase of u'/S_L from 1 to 3. Overall, the escalation of normalised turbulent flame speed is mostly due to the exaggerated flow pulsation instead of the increased heat release rate at elevated CO_2 wt.%. The use of biogas (CH_4/CO_2 mixture) to replace neat CH_4 for co-combustion with NH_3 is expected to incur intensified flow pulsation, the fluctuation intensity is likely to exacerbate as NH_3 wt.% in the biogas/NH_3 mixture is increased > 40%. There is a

503 lot of room for system optimisation going forward, especially with appropriate choice of swirl
504 number, preheating temperature, and elevated atmospheric pressure.
505
506

Acknowledgment

The authors gratefully acknowledge the funding support from the UCSI University through the Research Excellence & Innovative Grant (REIG-FETBE-2021/035).

References

[1] Valera-Medina A, Banares-Alcantara R, editors. Techno-Economic Challenges of Green Ammonia as an Energy Vector. Elsevier; 2021.

[2] The Royal Society. Ammonia : fuel and energy store 2020.

[3] Valera-Medina A, Xiao H, Owen-Jones M, David WIF, Bowen PJ. Ammonia for power. Prog Energy Combust Sci 2018;69:63–102. https://doi.org/10.1016/j.pecs.2018.07.001.

[4] Newhall HK, Starkman ES. Theoretical Performance of Ammonia as a Gas Turbine Fuel. SAE Trans 1967;75:772–84.

[5] Verkamp FJ, Hardin MC, Williams JR. Ammonia combustion properties and performance in gas-turbine burners. Symp Combust 1967;11:985–92. https://doi.org/10.1016/S0082-0784(67)80225-X.

[6] Kobayashi H, Hayakawa A, Somarathne KDKA, Okafor EC. Science and technology of ammonia combustion. Proc Combust Inst 2019;37:109–33.

[7] Valera-Medina A, Marsh R, Runyon J, Pugh D, Beasley P, Hughes T, et al. Ammonia–methane combustion in tangential swirl burners for gas turbine power generation. Appl Energy 2017;185:1362–71.

[8] Hayakawa A, Arakawa Y, Mimoto R, Somarathne KDKA, Kudo T, Kobayashi H. Experimental investigation of stabilization and emission characteristics of ammonia/air premixed flames in a swirl combustor. Int J Hydrogen Energy 2017;42:14010–8.

[9] Chiong MC, Valera-Medina A, Chong WWF, Chong CT, Mong GR, Mohd Jaafar MN. Effects of swirler vane angle on palm biodiesel/natural gas combustion in swirl-stabilised gas turbine combustor. Fuel 2020;277:118213. https://doi.org/10.1016/j.fuel.2020.118213.

[10] Chong CT, Chiong MC, Ng JH, Lim M, Tran MV, Valera-Medina A, et al. Oxygenated sunflower biodiesel: Spectroscopic and emissions quantification under reacting swirl spray conditions. Energy 2019;178:804–13. https://doi.org/10.1016/j.energy.2019.04.201.

[11] Khateeb AA, Guiberti TF, Zhu X, Younes M, Jamal A, Roberts WL. Stability limits and NO emissions of technically-premixed ammonia-hydrogen-nitrogen-air swirl flames. Int J Hydrogen Energy 2020;45:22008–18. https://doi.org/10.1016/j.ijhydene.2020.05.236.

[12] Somarathne KDKA, Okafor EC, Sugawara D, Hayakawa A, Kobayashi H. Effects of

549 OH concentration and temperature on NO emission characteristics of turbulent non-
550 premixed CH 4 /NH 3 /air flames in a two-stage gas turbine like combustor at high
551 pressure. Proc Combust Inst 2020;000:1–8.
552 https://doi.org/10.1016/j.proci.2020.06.276.
553 [13] Okafor EC, Somarathne KDKA, Hayakawa A, Kudo T, Kurata O, Iki N, et al.
554 Towards the development of an efficient low-NOx ammonia combustor for a micro
555 gas turbine. Proc Combust Inst 2019;37:4597–606.
556 https://doi.org/10.1016/j.proci.2018.07.083.
557 [14] An Z, Zhang M, Zhang W, Mao R, Wei X, Wang J, et al. Emission prediction and
558 analysis on CH4/NH3/air swirl flames with LES-FGM method. Fuel
559 2021;304:121370. https://doi.org/10.1016/j.fuel.2021.121370.
560 [15] Zhang M, Wei X, Wang J, Huang Z, Tan H. The blow-off and transient characteristics
561 of co-firing ammonia/methane fuels in a swirl combustor. Proc Combust Inst
562 2021;38:5859–68. https://doi.org/10.1016/j.proci.2020.08.056.
563 [16] Afzanizam N, Tung C, Ng J, Tran M, Chyuan H, Valera-medina A. ScienceDirect
564 Experimental and numerical studies on the premixed syngas swirl flames in a model
565 combustor. Int J Hydrogen Energy 2019;44:24126–39.
566 https://doi.org/10.1016/j.ijhydene.2019.07.158.
567 [17] Turkeli-ramadan Z, Sharma RN, Raine RR. Two-dimensional simulation of premixed
568 laminar fl ame at microscale. Chem Eng Sci 2015;138:414–31.
569 https://doi.org/10.1016/j.ces.2015.08.026.
570 [18] Krieger GC, Campos AP V, Takehara MDB, Alfaia F, Veras CAG. Numerical
571 simulation of oxy-fuel combustion for gas turbine applications. Appl Therm Eng
572 2015;78:471–81. https://doi.org/10.1016/j.applthermaleng.2015.01.001.
573 [19] Mayr B, Prieler R, Demuth M, Hochenauer C. The usability and limits of the steady fl
574 amelet approach in oxy-fuel combustions 2015;90:1478–89.
575 https://doi.org/10.1016/j.energy.2015.06.103.
576 [20] Mayr B, Prieler R, Demuth M, Potesser M, Hochenauer C. CFD and experimental
577 analysis of a 115 kW natural gas fired lab-scale furnace under oxy-fuel and air – fuel
578 conditions. Fuel 2015;159:864–75. https://doi.org/10.1016/j.fuel.2015.07.051.
579 [21] Sidey J, Mastorakos E. Visualisation of turbulent swirling dual-fuel flames. Proc
580 Combust Inst 2017;36:1721–7.
581 [22] Verhoeven LM, Ramaekers WJS, Oijen JA Van, Goey LPH De. Modeling non-
582 premixed laminar co-flow flames using flamelet-generated manifolds. Combust Flame

2012;159:230–41. https://doi.org/10.1016/j.combustflame.2011.07.011.
[23] Najafi-yazdi A, Cuenot B, Mongeau L. Systematic definition of progress variables and Intrinsically Low-Dimensional , Flamelet Generated Manifolds for chemistry tabulation. Combust Flame 2012;159:1197–204. https://doi.org/10.1016/j.combustflame.2011.10.003.
[24] Oijen JA Van, Goey LPH De. Predicting NO Formation with Flamelet Generated Manifolds n.d.
[25] Evans MJ, Sidey JAM, Ye J, Medwell PR, Dally BB, Mastorakos E. Temperature and reaction zone imaging in turbulent swirling dual-fuel flames. Proc Combust Inst 2019;37:2159–66. https://doi.org/10.1016/j.proci.2018.07.076.
[26] Law CK. Combustion Physics. Cambridge University Press; 2006.
[27] Khalil AEE, Gupta AK. Flame fluctuations in Oxy-CO2-methane mixtures in swirl assisted distributed combustion. Appl Energy 2017;204:303–17. https://doi.org/10.1016/j.apenergy.2017.07.037.
[28] Vigueras-Zuniga MO, Valera-Medina A, Syred N, Bowen P. High Momentum Flow Region and Central Recirculation Zone Interaction in Swirling Flows. Ing Mec Technol Y Desarro 2014;4:195–204.
[29] Gülder ÖL. Contribution of small scale turbulence to burning velocity of flamelets in the thin reaction zone regime. Proc Combust Inst 2007;31 I:1369–75. https://doi.org/10.1016/j.proci.2006.07.189.
[30] Luca S, Attili A, Lo Schiavo E, Creta F, Bisetti F. On the statistics of flame stretch in turbulent premixed jet flames in the thin reaction zone regime at varying Reynolds number. Proc Combust Inst 2019;37:2451–9. https://doi.org/10.1016/j.proci.2018.06.194.